Analysis of Electrode Configurations for Measuring Cardiac Tissue Conductivities and Fibre Rotation

Analysis of Electrode Configurations for Measuring Cardiac Tissue Conductivities and Fibre Rotation

Barbara M. Johnston and Peter R. Johnston*

School of Science

Griffith University

Nathan

Queensland

Australia, 4111

Phone: 61–7–3735–7748

Fax: 61–7–3735–7656

E–mail: P.Johnston@griffith.edu.au

David Kilpatrick

Department of Medicine

University of Tasmania

GPO Box 252-34

Hobart

Tasmania

Australia 7001

June 20, 2006

*Author to whom correspondence should be addressed.

Abstract

This paper describes a multi-electrode grid, which could be used to determine cardiac tissue parameters by direct measurement. A two pass process is used, where potential measurements are made, during the plateau phase of the action potential, on a subset of these electrodes and these measurements are used to determine the bidomain conductivities. In the first pass, the potential measurements are made on a set of 'closely-spaced' electrodes and the parameters are fitted to the potential measurements in an iterative process using a bidomain model and a solver based on a modified Shor's r-algorithm. This first pass yields the extracellular conductivities. The second pass is similar except that a 'widely-spaced' electrode set is used and this time the intracellular conductivities are recovered. In addition, it is possible to determine the fibre rotation throughout the tissue, since the bidomain model used here is able to include the effects of fibre rotation.

In the simulation studies presented here, the model is solved with known conductivities, on each of the two subsets of electrodes, to generate two sets of 'measured potentials'. Conductivities are then recovered by solving an inverse problem based on the measured potentials, to which various levels of noise are added. For example, simulations in the first pass are performed using an electrode spacing of 500 μm, for a situation where the longitudinal and transverse space constants are 769 μm and 308 μm respectively. These give very accurate average percentage relative errors for the longitudinal and

transverse extracellular conductivities, over five simulations with 1% noise added, of 0.3% and 0.2%. Twenty-five second pass simulations, on a 1 mm grid, yield average percentage relative errors of 3.8%, 2.6% and 1.4% for the corresponding intracellular values and the fibre rotation angle respectively.

Keywords: Bidomain model, anisotropy, conductivity values, electrodes, fibre rotation, simulation.

1 Introduction

Although the importance of obtaining measurements of cardiac tissue parameters, such as longitudinal and transverse conductivities, has long been recognised [1], few direct measurements have actually been made [2, 3, 4]. In addition, those parameters found in an indirect fashion [5, 6, 7], produce considerably different results when used to model situations such as ST segment shift in subendocardial ischaemia [8, 9], since they vary markedly [10] in value. This variation is not unexpected, given that each of the studies is conducted under particular experimental conditions and different modelling assumptions are used to interpret the results [11, 12, 13].

Since cardiac tissue anisotropy arises not only because of the different electrical conductivity along and across the cardiac fibres and within each of the intracellular and extracellular (interstitial) cardiac tissue spaces, but also because

of the rotation of the layers of cardiac fibres between the epicardium and the endocardium, it is also desirable to be able to determine the cardiac tissue fibre rotation. This has usually been found from detailed morphological studies [14] or by slicing away the fibres layer by layer [15], both of which are difficult and time-consuming.

The basis of most of the electrode systems [2, 3, 4, 16, 17, 18, 19] that are proposed to measure cardiac conductivities, is the four-electrode technique [20, 11], where current is applied to the outer pair of four equally spaced linear electrodes and potential is measured at the inner pair of electrodes. The studies by van Oosterom *et al.* [2] and Steendijk *et al.* [3] differ from the other work cited above, in that, although the cardiac tissue is taken to be anisotropic, it is treated as a monodomain rather than a bidomain. However, for some time, the bidomain model has been accepted as the most appropriate way to model electrical activity in cardiac tissue [12].

Plonsey and Barr [11] showed analytically for the case of equal anisotropy ratios, that current flows almost exclusively in the extracellular space when the electrode spacing is smaller than the space constant, whereas for much larger electrode spacings, some of the current is redirected into the intracellular space. This led to the proposal that in order to determine all the conductivities, measurements must be made along each of the axes (longitudinal and transverse), first using a ‘closely-spaced’ electrode and then using a ‘widely-spaced’ electrode,

where these electrode spacings correspond to the two scenarios mentioned above [11, 21, 18].

Le Guyader *et al.* [17] extended the ideas of Plonsey and Barr [11] by using a surface probe consisting of two orthogonal rows of four electrodes [16] with an electrode spacing of the order of the space constant, in conjunction with an AC current. In this case, a fraction of the current is redirected from the extracellular domain into the intracellular domain by increasing the frequency of the injected AC current. The cardiac tissue parameters were then calculated using a minimisation procedure, consisting of a first pass to fit the extracellular conductivities, followed by a second pass to fit the remainder of the parameters. The results presented did not include the effect of adding noise to the simulated potentials from which the parameters are recovered.

Barr and Plonsey [18] have proposed the use of a single perpendicularly inserted probe rather than a surface probe. This probe contains a mixture of extracellular electrodes and optical transmembrane potential sensors, which could be used to determine cardiac conductivity as well as membrane resistance. Both 'closely-spaced' and 'widely-spaced' sets of electrodes are used to find these parameters. More recently, Pollard *et al.* [19] showed that it is necessary to use both of these types of electrode separations to find intra- and extracellular myocyte conductivities in a single cardiac fibre. In this work, mulitsite interstitial stimulation was used along with one dimensional models based on the Luo-Rudy dynamic

membrane equations [22]. This work has been extended to use two-dimensional models [23].

Possible practical difficulties associated with these systems include the requirement for tiny electrodes and micrometre electrode spacings [18] and the precision required in manufacturing and calibrating these small electrode systems [19]. It has previously been demonstrated, by Hofer *et al.* [24] and Kim *et al.* [25], that it is possible to use microfabricated arrays to record electrograms in superfused guinea pig and perfused mouse and rabbit papillary muscle preparations. Recently, Wiley *et al.* [26] have measured surface potential components in perfused rabbit ventricular free wall epicardium, again using microfabricated sensors. The inter-electrode spacing used was 75 μm and this was systematically compared with recordings from arrays built from chloridised silver wire electrodes of either 50 μm or 250 μm diameters, with wider electrode spacing. Such studies suggest that the use of microfabricated arrays with micrometre spacing is technically feasible [23].

In order to recover the cardiac parameters from potential measurements, it is necessary to use a cardiac tissue model. This paper makes use of a previously presented [27] mathematical bidomain model, which is able to include the effects of fibre rotation. The model, which is solved using Fourier series and a simple one-dimensional finite difference scheme, is used to produce potential values on a particular multi-electrode grid. Once noise is added to these values, the cardiac

tissue fibre rotation and conductivities are recovered using an inversion technique, based on an extension of Tikhonov regularisation to non-linear problems [28] and on a modified Shor's r-algorithm [29]. The design of this particular electrode configuration is also discussed in relation to other multi-electrode grids, which do not work as effectively when recovering the cardiac tissue parameters.

2 Model

2.1 Governing Equations

A bidomain model [30, 31, 32] is used to model cardiac tissue, which is represented by a block of length 2L in each of the x and y directions. The epicardium corresponds to the plane at $z = 0$ and the endocardium to the plane at $z = 1$. The endocardium is in contact with a volume of blood that extends to infinity in the positive z direction.

The bidomain equations for the intra- and extracellular potentials, ϕ_i and ϕ_e, respectively, are given by

$$\nabla \cdot (\mathbf{M}_i \nabla \phi_i) = \beta / R(\phi_i - \phi_e) \tag{1}$$

$$\nabla \cdot (\mathbf{M}_e \nabla \phi_e) = -\beta / R(\phi_i - \phi_e) - I_s \tag{2}$$

where β is the surface to volume ratio of the cells, R is the specific membrane resistance and I_s is the external current source per unit volume applied in the ex-

tracellular space. The model is able to include the effects of cardiac fibre rotation and these are represented in the particular form of the conductivity tensors $\mathbf{M}_e$ and $\mathbf{M}_i$, described below.

Finally, the blood is a source-free region, and so the electric potential, ϕ_b, in the blood, is governed by Laplace's equation

$$\nabla^2 \phi_b = 0. \tag{3}$$

2.2 Conductivity Tensor

In this model, four conductivity values, g_{il}, g_{it}, g_{el} and g_{et} are required to represent the electrical conductivity in the cardiac tissue, where current flows differently within the intracellular (i) and extracellular (e) domains and also either longitudinal(l) to or transverse (t) to the cardiac fibres. The assumption is made here that the conductivity in either direction transverse to the fibres (that is, in the y or z direction) is the same.

Another component of the anisotropy occurs because the layers of fibres rotate relative to one another between the epi- and the endocardium. This is modelled under the following assumptions: the cardiac fibre layers are parallel to the epicardium [15]; the fibres are aligned with the positive x-axis and rotate anticlockwise from the epi- to the endocardium and this rotation varies linearly with depth

[33]. Hence, the conductivity tensors are of the form

$$\mathbf{M}_q(x,y,z) = \begin{pmatrix} (g_{ql}-g_{qt})c^2+g_{qt} & (g_{ql}-g_{qt})cs & 0 \\ (g_{ql}-g_{qt})cs & (g_{ql}-g_{qt})s^2+g_{qt} & 0 \\ 0 & 0 & g_{qt} \end{pmatrix} \tag{4}$$

where $q = i$ or e, $c = \cos\alpha z$, $s = \sin\alpha z$ and α is the total fibre rotation angle through the tissue which lies between 0 and π radians [14].

2.3 Boundary Conditions

Equations (1), (2) and (3) are used together with the following set of boundary conditions to solve the model. Firstly, assume that the epicardium is insulated:

$$\text{at } z = 0; \frac{\partial\phi_e}{\partial z} = \frac{\partial\phi_i}{\partial z} = 0. \tag{5}$$

The following conditions come from the fact that, at the interface between the tissue and the blood, there is continuity of extracellular potential and current, but the intracellular space is insulated by the extracellular space [34]; that is,

$$\text{at } z = 1; \phi_e = \phi_b, g_b\frac{\partial\phi_b}{\partial z} = g_{et}\frac{\partial\phi_e}{\partial z}, \frac{\partial\phi_i}{\partial z} = 0. \tag{6}$$

Then, since the blood mass is assumed infinite in the positive z-direction, $\phi_b \to 0$ as $z \to \infty$. In addition, assuming that the boundaries of the domain are insulated leads to the conditions that the derivatives of ϕ_e, ϕ_i and ϕ_b in the x and y directions are zero at the x and y boundaries.

2.4 Solution Method

Equations (1), (2) and (3), subject to boundary conditions (5) and (6), are solved using a Fourier Series approach, followed by a simple one-dimensional finite difference method. First, assume ϕ_e and ϕ_i are given by

$$\begin{aligned}\phi_q(x,y,z) = &\sum_{n=0}^{\infty}\sum_{m=0}^{\infty} C^q_{nm}(z)\cos m\pi y \cos n\pi x + D^q_{nm}(z)\sin m\pi y \cos n\pi x \\ &+ E^q_{nm}(z)\cos m\pi y \sin n\pi x + F^q_{nm}(z)\sin m\pi y \sin n\pi x\end{aligned} \tag{7}$$

for q=i or e. Substituting these into the differential equations gives two sets of four ordinary differential equations in z for the coefficients $C^q_{nm}(z)$, $D^q_{nm}(z)$, $E^q_{nm}(z)$ and $F^q_{nm}(z)$. Applying a one dimensional finite difference scheme, gives a banded system of linear algebraic equations that are solved numerically for the coefficients using standard techniques [35]. The series is then summed (here to 200 terms for both n and m) to give the potentials. Full details of the solution method can be found in [27]. This method has the advantage, over a Fourier Transform [17] or full numerical approach, that the potentials are calculated only at points, such as the measuring electrodes, where they are required, rather than at all the points on the structured grid defining the model geometry.

2.5 Modelling Parameters

The simulations presented here use a nominal set of conductivity values, based on the mean value of g_{il} calculated from the data of Clerc [5], Roberts *et al.* [6]

and Roberts and Sher [7], is used. These conductivity values are found using Roth's [10] recipe and are: $g_{il} = g_{el} = 0.0026$ S/cm, $g_{it} = 0.00026$ S/cm and $g_{et} = 0.00104$ S/cm. Again details can be found in [27]. Weidmann's [36] value of β=2000 cm^{-1} is used, along with Plonsey and Barr's [11] value for R of 9100 Ω cm^2. Based on these values, the longitudinal and transverse space constants are 769 μm and 308 μm respectively. In addition, an applied current of 50 μA is used, the conductivity of blood, g_b, is taken to be 0.0067 S/cm, the fibre rotation angle, α, is set to $2\pi/3$ radians and the block of tissue modelled is 2 cm by 2 cm (that is, L=1) and 1 cm thick.

3 Methods

A set of 'measured potentials' is produced here using a particular electrode array and the set of nominal values, for conductivities and fibre rotation, from Section 2.5, and this set is used to test the inversion process that will attempt to recover the original conductivity and fibre rotation parameters. It was found that the best results could be obtained using a two pass process, consisting of measurements made on a 'closely-spaced' grid, which are used to find the extracellular conductivities, followed by measurements made on a 'widely-spaced grid', which are used to refine the intracellular and fibre rotation values, found initially in the first pass.

3.1 Inversion Process

The idea of the method presented in this paper is to determine cardiac conductivity parameters and fibre rotation from measurements of certain potential differences. However, the forward model presented in the previous section suggests that the potentials depend non-linearly on the required parameters, of the form

$$\mathbf{G}(\mathbf{m}) = \mathbf{\Phi} \tag{8}$$

where $\mathbf{m}$ is the vector of required parameters and $\mathbf{\Phi}$ is the vector of measured voltages. $\mathbf{G}$ represents the forward model.

One way to obtain the vector $\mathbf{m}$ from a knowledge of the vector $\mathbf{\Phi}$ is to minimise the quantity

$$||\mathbf{G}(\mathbf{m}) - \mathbf{\Phi}||_2 \tag{9}$$

in the least squares sense. This method works provided that there is no noise in the measurement of the vector $\mathbf{\Phi}$. In a realistic measurement scenario, this would not be the case and noise would be present. To overcome this problem, it is necessary to minimise the Tikhonov functional [28]

$$||\mathbf{G}(\mathbf{m}) - \mathbf{\Phi}||_2^2 + \gamma^2||\mathbf{m}||_2^2 \tag{10}$$

where γ is the regularisation parameter. This functional weights the residual errors $||\mathbf{G}(\mathbf{m}) - \mathbf{\Phi}||_2$ against the actual size of the solution through the regularisation parameter.

For the specific problem being considered here, the Tikhonov functional to be minimised for the first pass through the solver is given by

$$f_1 = \sum_{i=1}^{16} \left[\phi_M(i) - \phi_C(i)\right]^2 + {\gamma_1}^2 \left[g_{il}^2 + g_{it}^2 + g_{el}^2 + g_{et}^2\right] + {\gamma_2}^2\alpha^2 \qquad (11)$$

where ϕ_M is the potential difference between the potential measured at electrode i and the reference electrode and ϕ_C is the potential difference between the potential calculated at electrode i and the reference electrode. The vector $\mathbf{m}$ is defined as $\mathbf{m} = [g_{il}, g_{it}, g_{el}, g_{et}, \alpha]^T$ and, due to the different orders of magnitude of the conductivities, $O(10^{-3})$, and the fibre rotation, $O(1)$, two different regularisation parameters, one of which is three orders of magnitude larger than the other, are utilized. Numerical experimentation has shown that the accuracy of the minimum of this functional is relatively insensitive to the values of γ_1 and γ_2. It was found that choosing $\gamma_1 = 10^{-2}$ and $\gamma_2 = 10^{-5}$ provided consistent results, when the units of conductivity are in S/cm, the potentials are measured in volts and the units of the fibre rotation angle α are radians. This function is minimised subject to the constraints that $0 \leq \alpha \leq \pi$ and $g_{il}, g_{it}, g_{el}, g_{et} > 0$.

A slightly different objective function, f_2, is used for the second pass through the solver, because g_{el} and g_{et} are held constant and g_{il} and g_{it} and α are allowed to vary:

$$f_2 = \sum_{i=1}^{18} \left[\phi_M(i) - \phi_C(i)\right]^2 + {\gamma_1}^2 \left[g_{il}^2 + g_{it}^2\right] + {\gamma_2}^2\alpha^2 \qquad (12)$$

In each case i is summed over the number of measuring electrodes in the grid (see

below).

Minimisation of the functionals f_1, equation (11), and f_2, equation (12), is performed using the SolvOpt solver [29], which minimises non-linear multivariate functions using a modified Shor's r-algorithm. The termination criterion used here is that the relative error in the value of f_1 (or f_2) obtained in two successive iterations is less than 10^{-6} [29]. The minimisation procedure yields values for the conductivities g_{il}, g_{it}, g_{el} and g_{et} and the fibre rotation angle α.

3.2 Electrode Array

The electrode array used here consists of 17 vertical probes, each containing two electrodes, so that two 'layers' of electrodes are formed, one at $z = 0.03$ and one at $z = 0.06$ cm, as shown in cross-section in Figures 1(a) and (b) or Figures 2(a) and (b). The array is aligned in the longitudinal and transverse directions as shown. A subset of 18 of these 34 electrodes, as shown in Figure 1, is used in the first pass to produce the first set of 'measured potentials'. This grid uses a spacing of 500 μm between pairs of electrodes in each layer and if the current source is regarded as being at the position $(0, 0, 0.03)$ cm, then the sink is at $(0.05, 0.05, 0.06)$ cm. A different subset of 20 of the electrodes is used for the second pass of the process; within each layer the measuring electrodes are 1000 μm = 1mm apart and the source and sink are at $(-0.05, -0.05, 0.03)$ cm and $(0.05, 0.05, 0.06)$ cm

respectively.

3.3 First Pass

The 'closely-spaced' electrode configuration, described in Section 3.2, is used, in conjunction with the set of nominal conductivities from Section 2.5 and a value of $2\pi/3$ for the fibre rotation, to produce a set of 'measured potentials' at the electrodes shown in Figure 1. Before applying the inversion process to attempt to recover these starting values, noise is added to the potential measurements. The five parameters $g_{il}, g_{it}, g_{el}, g_{et}$ and α are fitted simultaneously in the first pass through the solver, using f_1 from equation (11) with starting values of 1×10^{-3} for g_{il}, g_{el} and g_{et}, 1×10^{-4} for g_{it} and 0.5 for α.

3.4 Second Pass

Next the 'widely-spaced' grid, shown in Figure 2, is used in conjunction with the conductivities and value of fibre rotation from Section 2.5, to produce a second set of 'measured potentials' to which noise is added before the inversion process takes place. In this case, the values found for g_{el} and g_{et} from the first pass through the solver are now fixed and the SolvOpt [29] algorithm is used with f_2 from equation (12) to fit only the g_{il}, g_{it} and α values. The final values for these parameters from the first pass are used as starting values for the second pass.

3.5 Percentage Relative Error

The parameters, p_C, found by the inversion process, are compared with those parameters, p, in the generating set, by means of the percentage relative error defined by

$$\text{Percentage Relative Error} = \left| \frac{p - p_C}{p} \right| \times 100\% \tag{13}$$

where the parameters, p, are the nominal conductivity and the fibre rotation angle values given in Section 2.5.

4 Results

4.1 First Pass

The 'closely-spaced' electrode configuration, described in Section 3.2 and shown in Figure 1, is used, in conjunction with the set of conductivities given in Section 2.5, plus a value of $2\pi/3$ for the fibre rotation angle, to generate a set of 'measured potentials'. Random noise of 1%, 2% or 5% is added to these values and the inversion technique of Section 3.1 is used to recover all four conductivity values and a value for the fibre rotation angle. These values are compared with the original values by means of the percentage relative error, defined in Section 3.5. Then the percentage relative error for each parameter is averaged, over the five inversions which correspond to recovering the parameters when different starting potentials

are generated by randomly adding a particular amount of noise to the 'measured potentials'.

These average relative errors are given in Table 1 for g_{el} and g_{et} only and in Table 2, in the rows for grid spacing 500 μm, for all the parameters. The recovered extracellular values are very accurate, with average percentage relative errors that are considerably less than the noise added. In particular, for 1% noise, very accurate values of 0.3 and 0.2 $\%$ average relative errors for g_{el} and g_{et} are found.

Typical plots of percentage relative error for the extracellular conductivity values, intracellular conductivity values and the fibre rotation angle versus the iteration number in the SolvOpt routine [29], for 1% noise added, are shown in Figures 3, 4 and 5, respectively. In this example, the first pass consists of 56 iterations (Figure 3, first part of Figures 4 and 5), followed by a second pass of 24 iterations (second part of Figures 4 and 5). It can be seen that the percentage relative error for the extracellular conductivities (Figure 3) becomes less than the noise added before about half of the total number of iterations required to recover all five of the parameters and converges to consistent values after about 45 iterations. This is also true for the intracellular conductivities (Figure 4) and the fibre rotation angle (Figure 5), except that the values for g_{il} and g_{it} are less accurate than those for g_{el} and g_{et}, as can be seen in Table 2. However, these are good starting values for the second pass through the solver, as is the fibre rotation value.

4.2 Second Pass

Next the 'widely-spaced' electrode set, described in Section 3.1 and shown in Figure 2, is used to generate a second set of 'measured potentials', to which random noise is added. A second pass through the solver, using the method described in Section 3.3, then refines the values for the intracellular conductivity and fibre rotation angle, found in the first pass. This is demonstrated in the second part of Figures 4 and 5, where the relative errors drop between the start and end of the second pass. Figure 5 for the fibre rotation angle is atypical in that there is very little improvement in the relative error between the first and second pass; this is probably due to the fact that, in this particular simulation, the fibre rotation angle has already been recovered very accurately in the first pass. Note that the jump in the values of g_{il} and g_{it} at iteration 57 is related to the start of the second pass and is not significant.

For each category of noise, 1%, 2% or 5%, the five first pass runs are used as input for five new second pass runs, corresponding to adding this amount of noise, so the percentage relative error is averaged over 25 runs in this case. Results can be found in Table 1 for g_{il}, g_{it} and α. A comparison of the first pass values for these parameters, which can be found in Table 2 (for 500μm grid spacing) with the second pass values in Table 1, shows a considerable improvement from the first to the second pass for all the parameters; for example, the average percentage

relative error for g_{il} improves from 24.3 $\%$ to 9.1 $\%$ for the 2$\%$ noise case.

It is clear however, from Table 1, that the intracellular conductivities are more susceptible to noise than the extracellular conductivities and that the fibre rotation angle falls somewhere between these two categories in terms of the ease with which it can be recovered from the measured potentials.

4.3 Electrode Spacing

In addition to presenting the average percentage relative errors found in the first pass, as discussed in Section 4.1, Table 2 also contains the same type of information for the situation where the grid spacing within each layer of Figures 1(a) and (b) is now 250 μm instead of 500 μm. The idea here is to see if using a smaller grid spacing would improve the values found for the extracellular potentials.

In fact, the change to the closer electrode spacing does not appear to have much effect on the extracellular conductivities, as there is no change to the percentage relative errors for 1$\%$ noise, and for the other noise categories, an increase in the percentage relative error for one parameter corresponds to a decrease for the other parameter.

As would be expected, the errors for the intracellular potentials are considerably higher for the 250 μm grid than the 500 μm grid, since the former gird spacing corresponds to the situation where the electrode spacing is smaller than

the space constant (see Section 2.5) and therefore almost all the current is moving in the extracellular space [11]. Finally, the situation for the fibre rotation seems to indicate that the errors for the fibre rotation angle are generally lower or the same for the 500 μm grid as for the 250 μm grid.

5 Discussion

5.1 Electrode Configurations

This paper has presented two sets of electrode configurations, contained within the one array of electrodes, and a method describing how they can be used to recover the four cardiac tissue conductivities and the fibre rotation angle from voltage measurements at the electrodes. The grid consists of 17 dual-electrode probes, which are placed 500 μm apart. Different subsets of these electrodes are used in making the measurements; a 'closely-spaced' subset with electrode spacing 500 μm (Figure 1) and a 'widely-spaced' subset with electrode spacing 1 mm (Figure 2). These electrode configurations were chosen, after extensive testing of alternate electrode placements, as being those that best recovered the set of initial parameters, based on minimising the relative error of the difference between the initial and recovered values of the parameters. The reason for setting up the grid in this fashion was so that it could be built as one unit and therefore inserted into

the the tissue only once, but could produce results for both intra- and extracellular conductivities.

During this testing it was found that it appears to be necessary to make measurements on multiple probes in order to generate sufficient data for the inversion process to work, as various other electrode arrangements, such as, for example, multiple electrodes on two probes or even two sets of dual-electrode probes, arranged in an 'L' shape rather than a full grid, did not recover the parameters with sufficient accuracy.

5.2 Source and Sink Electrodes

Another aspect of the grid chosen is the choice of placement of the source and sink electrodes. Again, many different placements were investigated and the choices shown in Figures 1 and 2 were found to produce the best results. Notice that in each case, the source and sink are placed at different vertical heights (that is, one in each layer 300 μm apart) and that they are not placed on the one probe. This is so that both the longitudinal and transverse conductivities can be picked up because the source and sink are not aligned along either of those two directions. Also, because it is desired to recover the fibre rotation angle as well, the source and sink cannot be on the one probe as the potentials measured on a single probe are not affected by changes in fibre rotation angle [27].

Another point relates to the magnitude of the current applied. It was found that applying a current of 50 μA with the grid used here, as opposed to 5μA used by Barr and Plonsey [18], allows much more accurate recovery of the original parameters, since it reduces the relative noise levels. Although the 50 μA current is just above the threshold for action potential generation [21], it is possible to make the measurements during the action potential plateau phase, which limits the possibility of inducing an active response [19].

5.3 Choice of Electrode Spacings

Based on the analytic work of Plonsey and Barr [11], who studied current flows using the four-electrode technique for a scenario with an equal anisotropy ratio, it might have been thought that it would be necessary to use a 'close' electrode spacing which is less than the space constant. This is because this scenario corresponds to current flowing almost entirely in the extracellular space and this would presumably facilitate the recovery of the extracellular conductivities from the potential measurements.

Before choosing the electrode spacing it is instructive to examine the values for the space constant for the various published values for the cardiac conductivities. These can be found in Table 3 where the values from Section 2.5 for R and β have been assigned to the first three authors for the purpose of comparison, since the

values are not available in these cases. There is a considerable variation in both the longitudinal value, λ_l, from 471 to 1052 μm and in the transverse value, λ_t, from 196 to 439 μm. However, the value of the ratio λ_l/λ_t is consistently around 2.5, except for the work of Roberts and Sher [7]. Note that this ratio is independent of the values of R and β since these parameters cancel out in the ratio. It can be seen that the 'close' electrode spacing of 500 μm used here falls between the the values of the longitudinal and transverse space constants of 769 μm and 308 μm respectively and is thus of the same order as the space constant.

Consideration of the graphs of Plonsey and Barr [11] which show potential versus position for the three scenarios (a), (b) and (c), where the electrode spacing is respectively much less than, equal to and much greater than the space constant, reveals that the source and sink electrodes are placed at a distance of 2$\times$(space constant) apart and that the measuring electrodes are $\frac{2}{3}\times$(space constant) apart. This fits well with the placement of the source and sink in the array used here, since they are 768 μm apart compared with 2$\times$308=616 μm and 2$\times$769=1538 μm (see Table 3). So the measurements on the 500 μm grid are either (a) or (b) scenarios. Since in scenario (b) the current still flows mostly through the extracellular space [11], it is perhaps not so surprising that the extracellular conductivities can be recovered using a 500 μm electrode spacing, particularly bearing in mind that the potential measurements are being made on a far more complex grid than the usual four-electrode probe.

The second pass uses an electrode spacing within each layer of 1000 μm and this corresponds to the case of Plonsey and Barr [11] where the electrode spacing is much greater than the space constant. In this case the current is flowing in both the extracellular and intracellular spaces and therefore the potentials obtained may be sufficiently sensitive to changes in the intracellular conductivities to allow them to be recovered. This has proved to be the case, although the results have higher relative errors than for the extracellular conductivities. It might be thought that increasing the electrode spacing still further could produce better results for the intracellular conductivities, but this was not found, perhaps because the magnitude of the potentials drops for more widely spaced electrodes.

5.4 Limitations of the method

Fibre rotation throughout the tissue is modelled here under a number of assumptions: fibre rotation is assumed to vary linearly with depth; the imburcation angle, the angle of inclination of the fibres relative to the epicardial surface, is assumed to be zero (these are both reasonably common modelling assumptions [33]); the fibre sheets are assumed to be parallel with the epicardium. This means that the method is applicable at all points except near the apex and base of the heart [15]. Here, the intracellular conductivities do not include separate components for the myoplasmic and gap junction contributions to the conductivity and it is assumed

that the conductivities in the two transverse directions (y and z) are equal. In addition, the work presented here assumes that the grid can be placed in the tissue without causing significant injury currents [37] and that it is aligned with the longitudinal and transverse directions, as shown in Figures 1 and 2. This can be achieved using techniques published elsewhere [3, 6, 38].

5.5 Advantages of the proposed grid

Recently some authors have suggested using much smaller electrode spacings than those used here. For example, Barr and Plonsey [18] propose using a 'close' spacing of 50 μm and a 'wide' spacing of 200 μm for a vertical probe of total length 1 mm. In their scenario $\lambda_l = 1052\mu$m and $\lambda_t = 439\mu$m (see Table 3). They suggest that an advantage of such a small probe is that the assumption need only be made that the tissue is uniform over about 1 mm [18]. However, since the model being used here does include fibre rotation, such small electrode spacings are not necessary and, as discussed in Section 4.3, simulations using a smaller 250 μm spacing with the proposed grid do not produce lower relative errors for the extracellular conductivities.

Alternatively, there are advantages associated with using the wider 500 μm spaced grid proposed here. The wider electrode removes the necessity of fabricating arrays with very small electrode spacings and also any problems related to the

fact that such spacings are smaller than the length of cardiac cells (100-150 μm) [11], where the bidomain model may no longer be valid [21].

6 Conclusions

A multi-electrode grid, plus a method for using 'closely-spaced' and 'widely-spaced' subsets of these electrodes, has been proposed here, for use in determining intra- and extracellular cardiac tissue conductivities, as well as fibre rotation angle. These subsets correspond to inter-electrode spacings of 500 and 1000 μm respectively, compared with longitudinal and transverse space constants of 769 and 308 μm respectively. The cardiac parameters are found, from voltage measurements made on the grid, by applying an inversion technique based on Tikhonov regularisation and a modified Shor's r-algorithm.

In the simulations conducted here, a previously proposed bidomain model [27] which includes fibre rotation, is used with a set of nominal parameter values to generate a set of 'measured potentials', to which 1, 2 or 5$\%$ noise is added. The parameters are recovered in two passes; the first uses the 'closely-spaced' grid and recovers the extracellular conductivities and the second refines the intracellular conductivities and the fibre rotation, found initially in the first pass, using the 'widely-spaced' grid. The extracellular conductivities are recovered very accurately with average percentage relative errors generally around half or less than

the noise added; for example, for 1% noise , the average percentage relative errors are 0.3 and 0.2% for g_{el} and g_{et} respectively. The intracellular conductivities are more susceptible to noise than the extracellular conductivities, with average percentage relative errors generally lying between 2.5 and 4 times the added noise. It is also possible to recover the fibre rotation angle quite accurately, with average percentage relative errors of 1.4, 2.0 and 8.2% for 1, 2 and 5% noise respectively.

An extension of the model and the method, to include the use of an applied AC current, may also allow the determination of further cardiac parameters.

Acknowledgment

This work was funded by the Australian Research Council.

References

[1] B. J. Roth, "Mechanisms for electrical stimulation of excitable tissue," *Crit. Rev. Biomed. Eng.*, vol. 22, pp. 253–305, 1994.

[2] A. van Oosterom, R. W. de Boer, and R. Th. Van Dam, "Intramural resistivity of cardiac tissue," *Med. & Biol. Eng. & Comput.*, vol. 17, pp. 337–343, 1979.

[3] P. Steendijk, G. Mur, E. T. van der Velde, and J. Baan, "The four-electrode resistivity technique in anisotropic media: Theoretical analysis and application on myocardial tissue *in Vivo*," *IEEE Transactions on Biomedical Engineering*, vol. 40, no. 11, pp. 1138–1147, 1993.

[4] P. Le Guyader, P. Savard, and F. Trelles, "Measurement of myocardial conductivities with an eight–electrode technique in the frequency domain," *17th IEEE-EMBS*, pp. 71–72, 1995.

[5] L. Clerc, "Directional differences of impulse spread in trabecular muscle from mammalian heart," *Journal of Physiology*, vol. 255, pp. 335–346, 1976.

[6] D. E. Roberts, L. T. Hersh, and A. M. Scher, "Influence of cardiac fiber orientation on wavefront voltage, conduction velocity and tissue resistivity in the dog," *Circ. Res.*, vol. 44, pp. 701–712, 1979.

[7] D. E. Roberts and A. M. Scher, "Effects of tissue anisotropy on extracellular potential fields in canine myocardium in situ," *Circ. Res.*, vol. 50, pp. 342–351, 1982.

[8] Peter R. Johnston and David Kilpatrick, "The effect of conductivity values on ST segment shift in subendocardial ischaemia," *IEEE Transaction on Biomedical Engineering*, vol. 50, no. 2, pp. 150–158, February 2003.

[9] Peter R. Johnston, "A cylindrical model for studying subendocardial ischaemia in the left ventricle," *Mathematical Biosciences*, vol. 186, no. 1, pp. 43–61, 2003.

[10] B. J. Roth, "Electrical conductivity values used with the bidomain model of cardiac tissue," *IEEE Transactions on Biomedical Engineering*, vol. 44, no. 4, pp. 326–328, April 1997.

[11] R. Plonsey and R. C. Barr, "The four-electrode resistivity technique as applied to cardiac muscle," *IEEE Transactions on Biomedical Engineering*, vol. 29, no. 7, pp. 541–546, 1982.

[12] R. Plonsey and R. C. Barr, "A critique of impedance measurements in cardiac tissue," *Annals of Biomedical Engineering*, vol. 14, pp. 307–322, 1986.

[13] Jeroen Stinstra, Bruce Hopenfeld, and Rob MacLeod, "On the passive cardiac conductivity," *Annals of Biomedical Engineering*, vol. 33, no. 12, pp. 1743–1751, 2005.

[14] D. D. Streeter, "Gross morphology and fiber geometry of the heart," in *Handbook of Physiology, Vol 1*, R. M. Berne, Ed., chapter 2: The Cardiovascular System, pp. 61–112. Williams and Williams, Baltimore, MD, 1979.

[15] I. J. LeGrice, P. J. Hunter, and B. H. Smail, "Laminar structure of the heart: a mathematical model," *American Journal of Physiology*, vol. 272, pp. H2466–H2476, 1997.

[16] P. Le Guyader, P. Savard, R. Guardo, L. Pouliot, F. Trelles, and M. Meunier, "Myocardial impedance measurements with a modified four electrode technique," *16th IEEE-EMBS*, pp. 880–881, 1994.

[17] P. Le Guyader, F. Trelles, and P. Savard, "Extracellular measurement of anisotropic bidomain myocardial conductivities. I. Theoretical analysis," *Annals of Biomedical Engineering*, vol. 29, pp. 862–877, 2001.

[18] R. C. Barr and R. Plonsey, "Electrode systems for measuring cardiac impedances using optical transmembrane potential sensors and interstitial electrodes — Theoretical design," *IEEE Transactions on Biomedical Engineering*, vol. 50, no. 8, pp. 925–934, 2003.

[19] A. E. Pollard, W. M. Smith, and R. C. Barr, "Feasibility of cardiac microimpedance measurement using multisite interstitial stimulation," *Am J Physiol Circ Physiol*, vol. 287, pp. H2402–H2411, 2004.

[20] S. Rush, J. A. Abildskov, and R. McFee, "Resistivity of body tissues at low frequencies," *Circulation Research*, vol. 12, pp. 40–50, 1963.

[21] R. M. Gulrajani, *Bioelectricity and Biomagnetism*, John Wiley and Sons, 1998.

[22] T. J. Hund, J. P. Kucera, N. F. Otani, and Y. Rudy, "Ionic charge conservations and long-term steady state in the Luo-Rudy dynamic cell model," *Biophys J.*, vol. 81, pp. 3324–3331, 2001.

[23] A. E. Pollard and R. C. Barr, "Cardiac micro–impedance measurement in two–dimensional models using multisite interstitial stimulation," *American Journal of Physiology-Heart and Circulatory Physiology*, p. (in press), 2006.

[24] E Hofer, G Urban, M S Spach, I Schafferhofer, G Mohr, and D Platzer, "Measuring activation patterns of the heart at a microscopic size scale with thin-film sensors," *American Journal of Physiology*, vol. 266, no. 5, pp. H2136–H2145, May 1994.

[25] Chang-Soo Kim, Stefan Ufer, Christopher M. Seagle, Connie L. Engle, H. Troy Nagle, Timothy A. Johnson, and Wayne E. Cascio, "Use of micro-

machined probes for the recording of cardiac electrograms in isolated heart tissues," *Biosensors and Bioelectronics*, vol. 19, no. 9, pp. 1109–1116, Apr 2004.

[26] JJ Wiley, RE Ideker, WM Smith, and Pollard AE, "Measuring surface potential components necessary for transmembrane current computation using microfabricated arrays," *American Journal of Physiology-Heart and Circulatory Physiology*, vol. 289, no. 6, pp. H2468–H2477, Dec 2005.

[27] Barbara M. Johnston, Peter R. Johnston, and David Kilpatrick, "A new approach to the determinination of cardiac potential distributions: Application to the analysis of electrode configurations," *(Revised and resubmitted)*, 2006.

[28] R. C. Aster, B. Borchers, and C. H. Thurber, *Parameter Estimation and Inverse Problems*, Elsevier Academic Press, Burlington, 2005.

[29] A. Kuntsevich and F. Kappel, *SolvOpt: The solver for Local Nonlinear Optimisation Problems, version 1.1 in C*, Institute for Mathematics: Karl–Franzens University of Graz, 1997.

[30] L. Tung, *A Bi–domain model for describing ischaemic myocardial D-C potentials*, Ph.D. thesis, Massachusetts Institute of Technology, June 1978.

[31] W. T. Miller and D. B. Geselowitz, "Simulation studies of the electrocardiogram I: The normal heart," *Circulation Research*, vol. 43, pp. 301–315, 1978.

[32] O. H. Schmitt, "Biological information processing using the concept of interpenetrating domains," in *Information Processing in the Nervous System*, K. N. Leibovic, Ed., chapter 18, pp. 325–331. Springer–Verlag, New York, 1969.

[33] P. Colli-Franzone and L. Guerri, "Spreading of excitation in 3–D models of the anisotropic cardiac tissue I: Validation of the eikonal model," *Mathematical Biosciences*, vol. 113, pp. 145–209, 1993.

[34] W. Krassowska and J.C. Neu, "Effective boundary conditions for syncytial tissues," *IEEE Transactions on Biomedial Engineering*, vol. 41, no. 2, pp. 143–150, 1994.

[35] William H. Press, Brian P. Flannery, Saul A. Teukolsky, and William T. Vetterling, *Numerical Recipes, The Art of Scientific Computing*, Cambridge University Press, Cambridge, 2nd edition, 1992.

[36] S. Weidmann, "Electrical constants of trabecular muscle from mammalian heart," *J. Physiol.*, vol. 210, pp. 1041–1054, 1970.

[37] Q. Li, *Transmyocardial ST potential distributions in ischaemic heart disease,* Ph.D. thesis, University of Tasmania, 2005.

[38] Y. Wang, P. H. Schimpf, D. R. Haynor, and Y. Kim, "Geometric effects on resistivity measurements with four– electrode probes in isotropic and anisotropic tissues," *IEEE Transactions on Biomedical Engineering*, vol. 45, no. 7, pp. 8–19, July 1998.

Captions

Figure 1: Grid configuration, for the first pass, consisting of 9 dual-electrode probes, with an inter-electrode spacing of 500 μm within each of the (a) top and (b) bottom 'layers'. These 'layers' correspond to the electrodes placed at (a) $z = 0.03$ cm and (b) $z = 0.06$ cm. Current source and sink are indicated with a $+$ and $-$ respectively.

Figure 2: Grid configuration, for the second pass, consisting of 9 dual-electrode probes, with an inter-electrode spacing of 1000 μm within each of the (a) top and (b) bottom 'layers'. These 'layers' correspond to the electrodes placed at (a) $z = 0.03$ cm and (b) $z = 0.06$ cm. Current source and sink are indicated with a + and - respectively and are placed on additional probes.

Figure 3: A plot of the percentage relative error for the extracellular conductivities, g_{el} and g_{et}, versus the iteration number in the SolvOpt [29] inversion algorithm.

Figure 4: A plot of the percentage relative error for the intracellular conductivities, g_{il} and g_{it}, versus the iteration number in the SolvOpt [29] inversion algorithm, showing values from the first pass followed by values from the second pass.

Figure 5: A plot of the percentage relative error for the fibre rotation angle, α, versus the iteration number in the SolvOpt [29] inversion algorithm, showing values from the first pass followed by values from the second pass.

Table 1: Summary of average percentage relative errors for various noise levels when recovering the given cardiac parameters using a first pass for the extracellular conductivities and a second pass for the intracellular conductivities and the fibre rotation angle.

Table 2: A comparison of the percentage relative errors found when using a first pass to recover the given cardiac parameters using either a 250 μm or 500 μm electrode spacing in the grid.

Table 3: Longitudinal, λ_l, and transverse, λ_t, space constants (in microns) using conductivity values from various authors. Values of R=9100 Ω cm^2 and β=2000 cm^{-1} are assumed for the first three authors, since they are not available in these cases.

(a) z = 0.03 cm

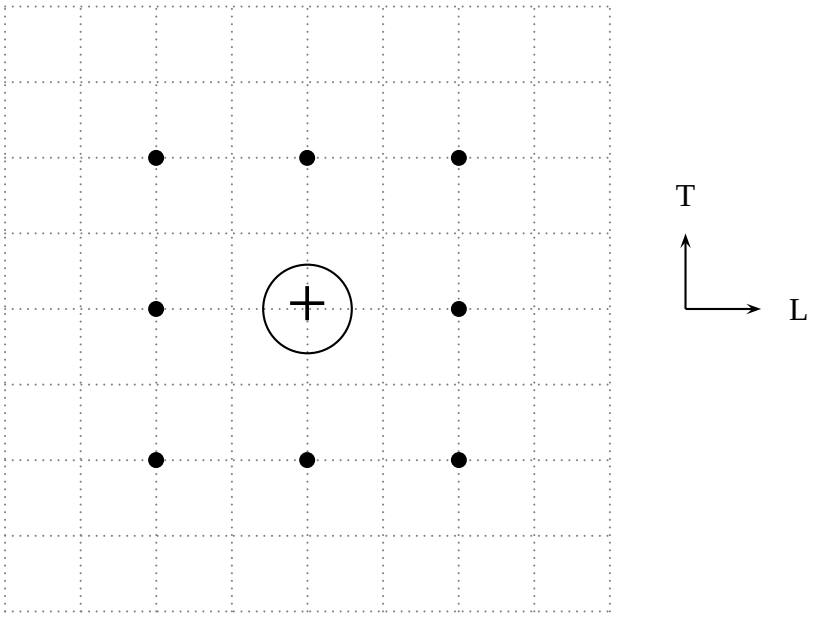

(b) z = 0.06 cm

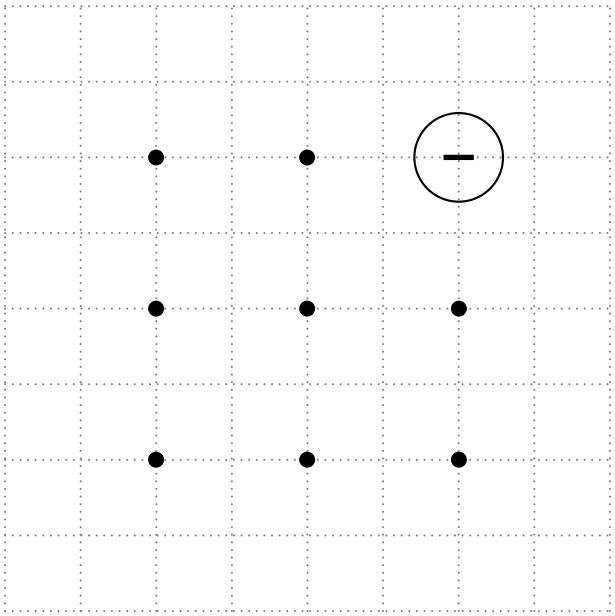

Figure 1:

(a) z = 0.03 cm

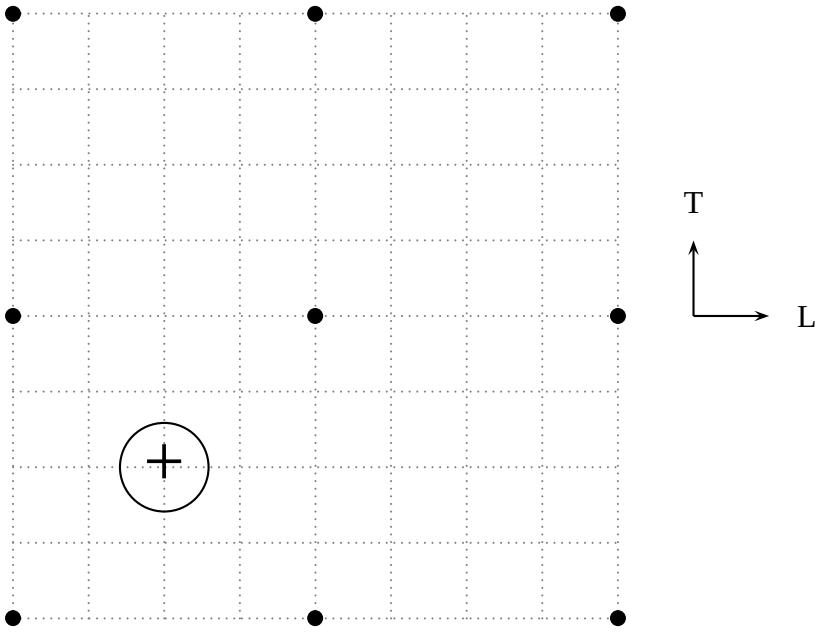

(b) z = 0.06 cm

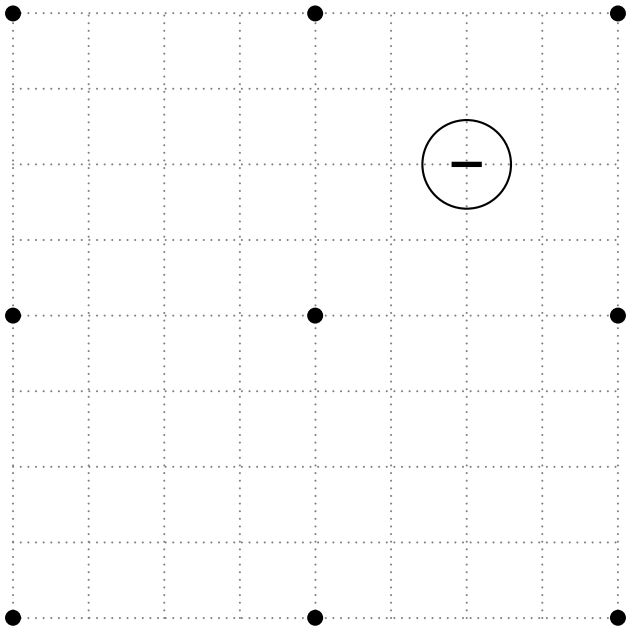

Figure 2:

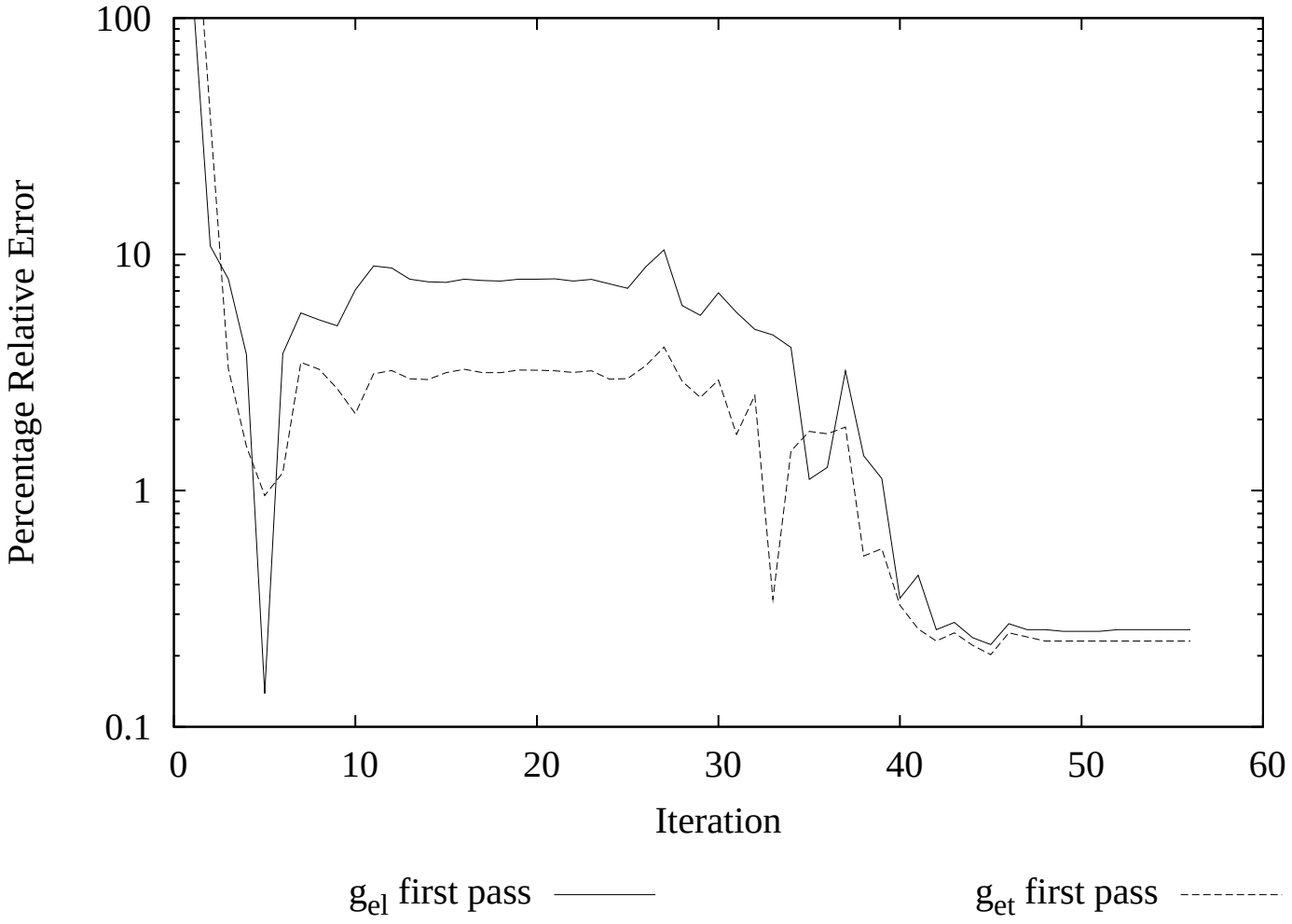
100
10
1
0.1
Percentage Relative Error
0
10
20
30
40
50
60
Iteration
g_{el} first pass
g_{et} first pass

Figure 3:

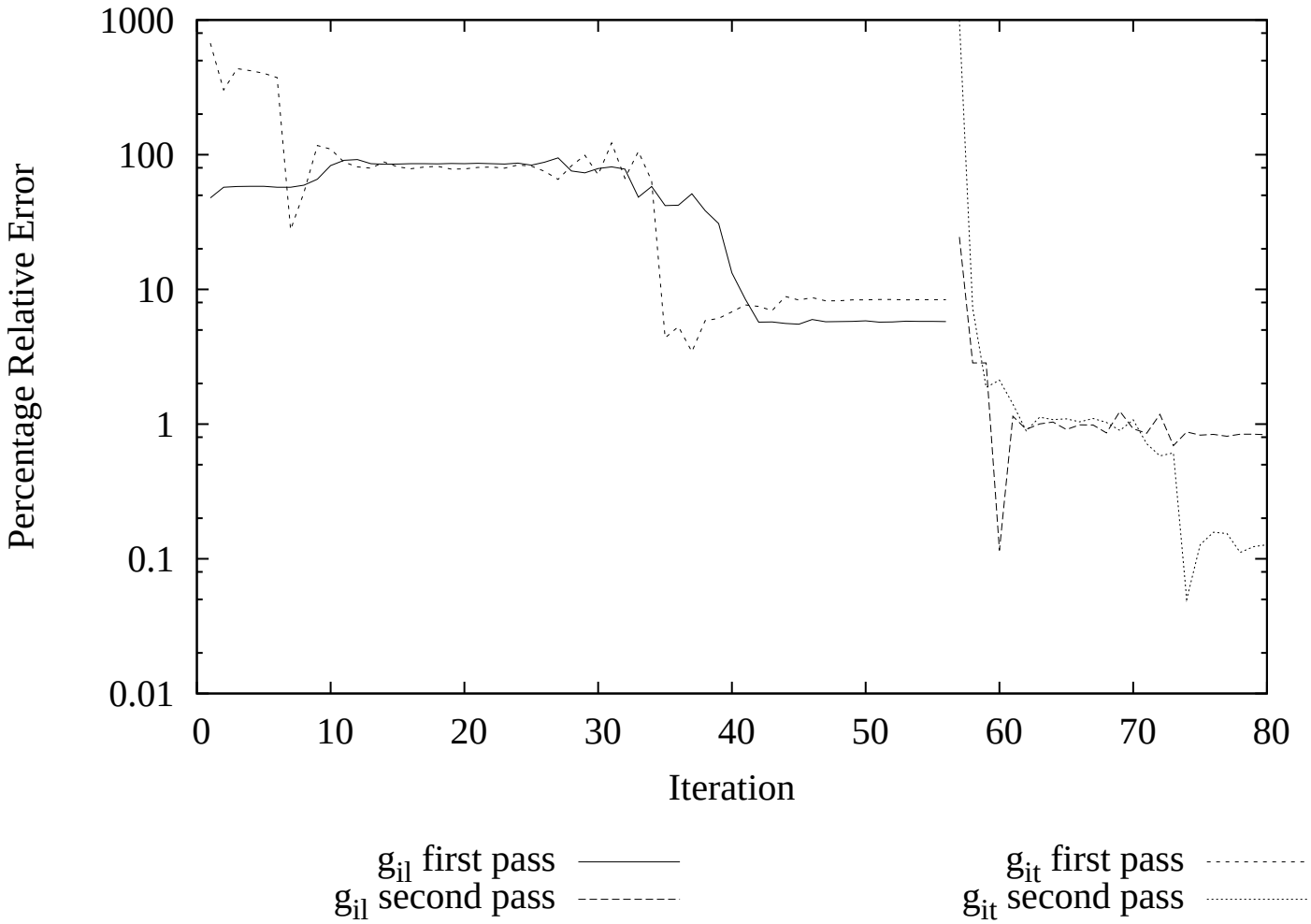
1000
100
10
1
0.1
0.01
Percentage Relative Error
0
10
20
30
40
50
60
70
80
Iteration
g_{il} first pass
g_{il} second pass
g_{it} first pass
g_{it} second pass

Figure 4:

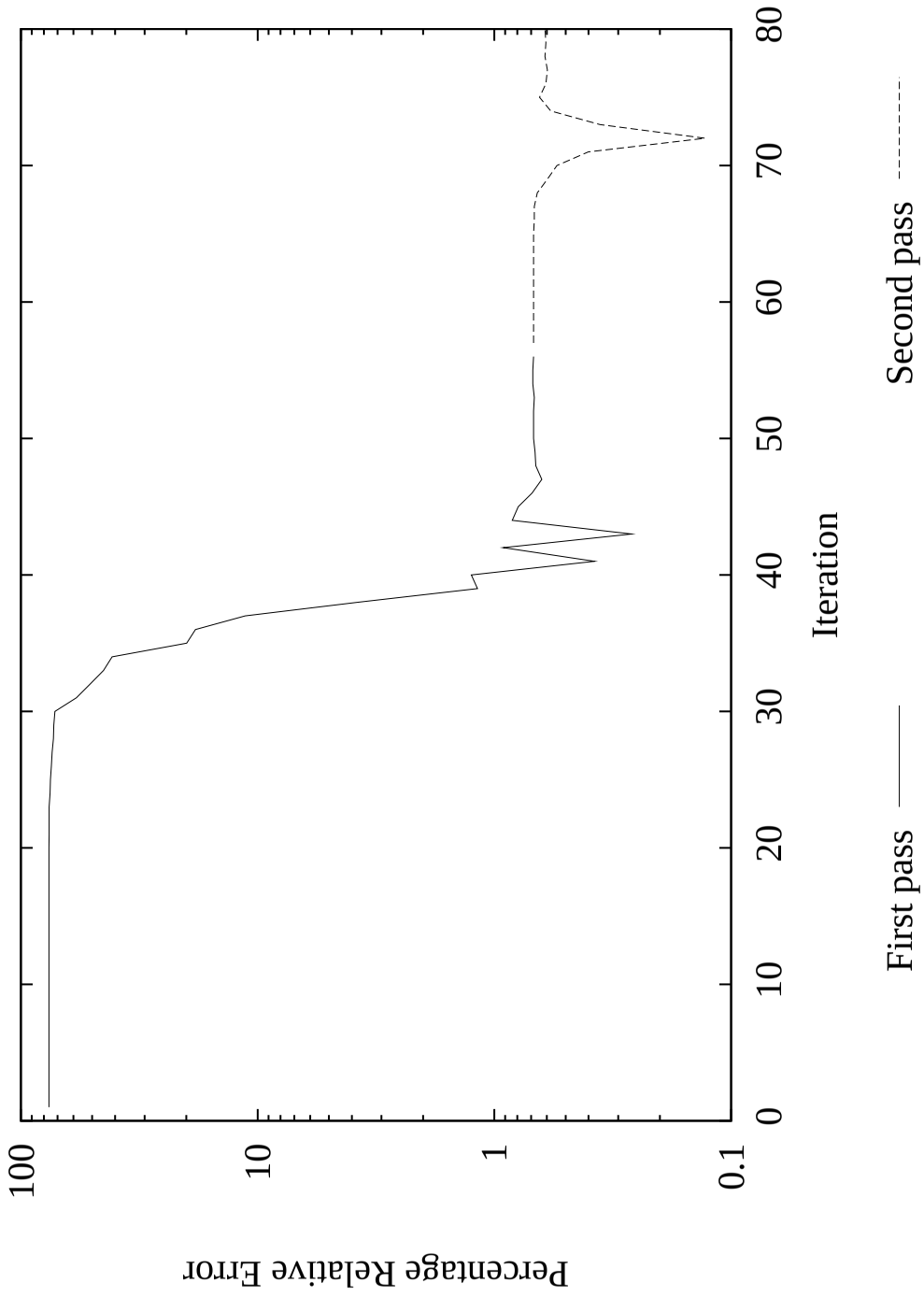
Percentage Relative Error
100
10
1
0.1
0
10
20
30
40
50
60
70
80
Iteration
First pass
Second pass

Figure 5:

Noise %	First Pass		Second Pass		
	g_{el}	g_{et}	g_{il}	g_{it}	α
1	0.3	0.2	3.8	2.6	1.4
2	1.3	0.6	9.1	5.1	2.0
5	2.9	2.5	19.3	16.0	8.2

Table 1:

Noise (%)	Grid Spacing (μm)	g_{el}	g_{et}	g_{il}	g_{it}	α
1	250	0.3	0.2	49.7	37.3	4.0
	500	0.3	0.2	7.3	5.4	2.2
2	250	0.8	0.7	339.0	59.1	4.5
	500	1.3	0.6	24.3	13.4	4.9
5	250	3.3	1.9	309.9	371.2	17.2
	500	2.9	2.5	25.2	28.8	12.0

Table 2:

	Clerc [5]	Roberts *et al.*[6]	Roberts and Sher[7]	Plonsey and Barr[11]	Le Guyader *et al.*[4]	Le Guyader *et al.*[17]	Barr and Plonsey[18]	Nominal [27]
λ_l	787	749	635	471	480	740	1052	769
λ_t	285	314	395	196	202	283	439	308
$\frac{\lambda_l}{\lambda_t}$	2.8	2.4	1.6	2.4	2.4	2.6	2.4	2.5

Table 3: